



Light-inducible control of cellular proliferation and differentiation by a Hedgehog signaling inhibitor

Ryuji Misawa^{a,c}, Tsuyoshi Minami^{a,c}, Akimitsu Okamoto^{b,c}, Yoshiho Ikeuchi^{a,c,*}

^a Institute of Industrial Science, The University of Tokyo, Tokyo 153-8505, Japan

^b Research Center for Advanced Science and Technology, The University of Tokyo, Tokyo 153-8505, Japan

^c Department of Chemistry and Biotechnology, The University of Tokyo, Tokyo 153-8505, Japan

ARTICLE INFO

Keywords:

Hedgehog signaling
Photo-caged compounds
Light therapy

ABSTRACT

The Hedgehog (Hh) signaling pathway is a major regulator of cell differentiation and proliferation. Aberrant activation of the Hh pathway has been implicated in several types of cancer. To understand the Hedgehog pathway and fight against related diseases, it is important to inhibit Hedgehog signaling in a targeted manner. However, no tools are available for the precise inhibition of Hh signaling in a spatiotemporal manner. In this study, we synthesized and evaluated the bioactivity of a light-inducible Hh pathway inhibitor (NVOC-SANT-75). NVOC-SANT-75 inhibits transcription factor Gli1 in NIH3T3 cells and controls proliferation and differentiation of primary cultured mouse cerebellar neurons in a light-irradiation-dependent manner. The light-inducible Hedgehog signaling inhibitors may be a new candidate for light-mediated cancer treatment.

1. Introduction

Cancer is one of the most significant public health challenges in this world. As our understanding of the molecular basis of cancer develops so our ability to produce novel anti-cancer agents targeting specific signaling pathways essential for cancer proliferation grows.¹ The Hedgehog (Hh) signaling pathway controls cell proliferation and differentiation, and hyperactivation of the Hh signaling pathway is associated with the pathogenesis of several cancers.^{2,3} Activation of the Hh signaling pathway is initiated by the binding of the Hh ligand to its receptor, Patched (Ptc).^{3,4} In the absence of the Hh ligand, Ptc constitutively inhibits the seven-transmembrane G protein-coupled receptor Smoothened (Smo). Binding of Hh ligand to Ptc results in the loss of this suppression, then Smo is trafficked to the primary cilia and activates the downstream signaling cascade, leading to the activation of the Gli transcription factors.

Mutations in Hh genes such as Ptc and Smo can cause heritable Hh-associated diseases. These mutation-driven Hh dependent cancers are ligand-independent. For example, Gorlin syndrome⁵ is caused by a loss-of-function mutation in the Ptc gene. Patients present with numerous basal cell carcinomas (BCCs) during their lifetime and are at an increased risk of medulloblastoma. Two Smo inhibitors, vismodegib and sonidegib, have been approved by the FDA and have been used to treat

BCC. An increasing number of Hh-associated tumors in a wide variety of organs, including the lung,⁶ esophagus,⁷ pancreas,⁸ prostate,⁹ breast¹⁰ and liver¹¹ have been found to be ligand-dependent tumors. In these tumors, the Hh signal is hyperactivated by increased paracrine and autocrine signaling resulting from increases in the prevalence of the Hh peptides.¹² Many other Smo inhibitors against ligand-dependent cancers are currently under clinical research.¹³ Smo inhibitors are administered to the entire body. However, systemic application of these drugs can result in unwanted side effects, limiting their maximum dosage and thus hindering their effectiveness. Therefore, there is an urgent need to develop more sophisticated technologies for precise inhibition of the Hh pathway in cancer.

“Caged” compounds show effective spatiotemporal control of biological processes.^{14,15} These compounds are produced by coupling biomolecules with a protecting group via a photo-cleavable bond. Upon light irradiation at a specific wavelength, the protecting group is removed, and the active substrate is released. We have developed a caged Hh signaling activator for controlling the dorsoventral differentiation of cerebral organoids in a previous study.¹⁶ Here, we synthesized and evaluated a Hh inhibitor for controlling cellular proliferation and differentiation using a similar strategy.

* Corresponding author.

E-mail address: yikeuchi@iis.u-tokyo.ac.jp (Y. Ikeuchi).

<https://doi.org/10.1016/j.bmc.2021.116144>

Received 22 December 2020; Received in revised form 22 March 2021; Accepted 28 March 2021

Available online 2 April 2021

0968-0896/© 2021 Elsevier Ltd. All rights reserved.

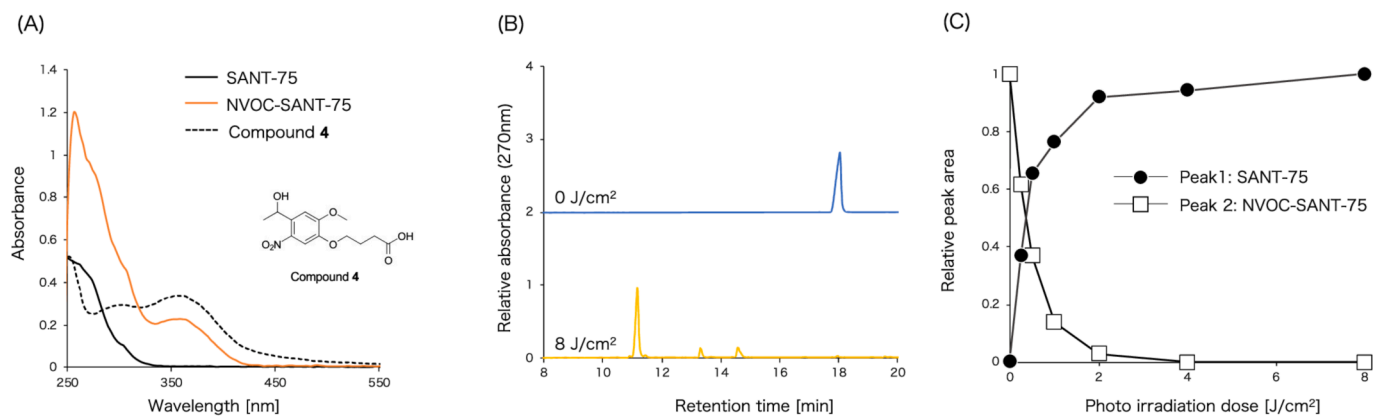


Fig. 1. Characterization of NVOC-SANT-75 decomposition in response to light exposure. (A) UV-Vis absorption spectra of SANT-75, NVOC-SANT-75 and compound 4. (B) Chromatogram profiles of photo-irradiated NVOC-SANT-75. Peak2 (18–19 min): NVOC-SANT75, Peak1 (11–12 min): SANT-75. Peak identities were determined by ESI-MS. (C) Photo-irradiation mediated decomposition was dose dependent as demonstrated by this decomposition curve.

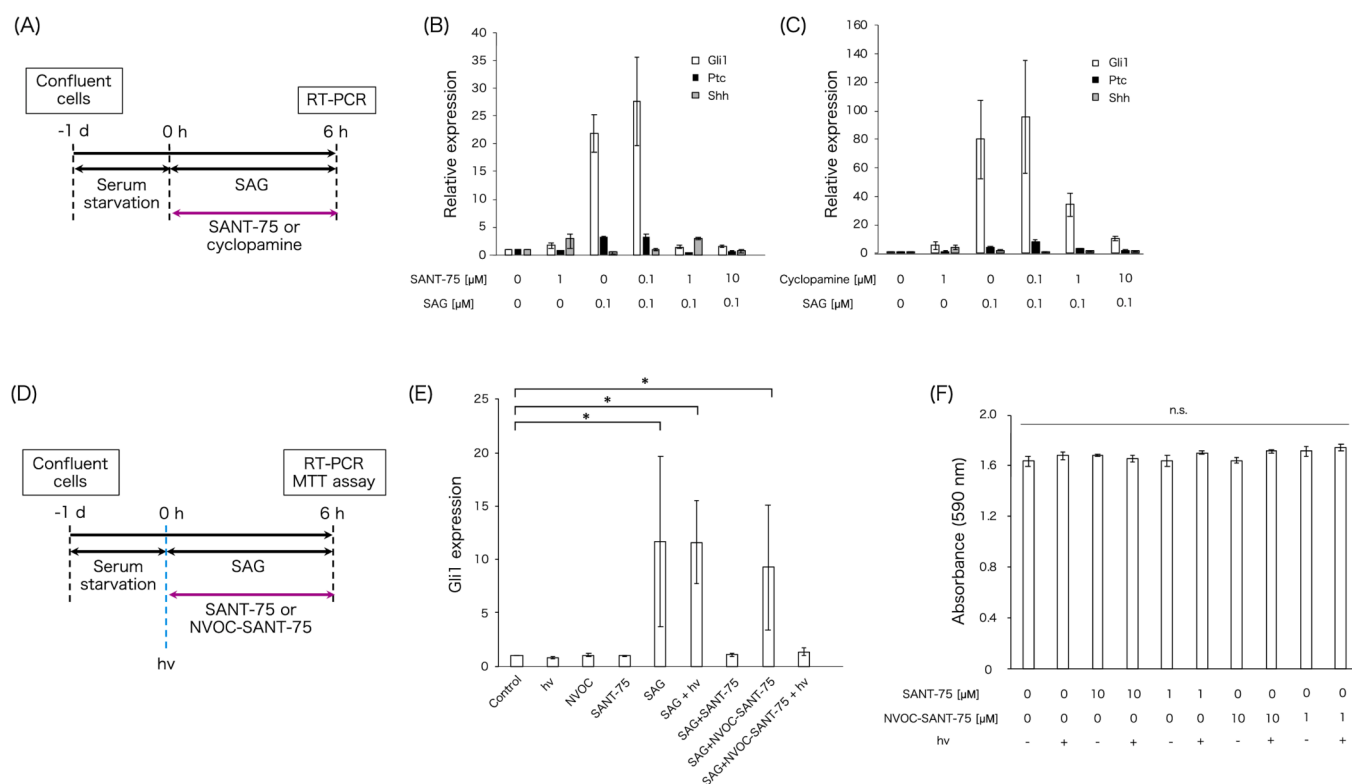


Fig. 2. Characterization of NVOC-SANT-75 using NIH3T3 cells. (A) Timeline of the experimental procedures used in (B) and (C). After 1 day of starvation, medium was changed to fresh starvation medium supplemented with SAG or Hh inhibitors (SANT-75 and cyclopamine). (B) Relative expression levels of *Gli1*, *Ptc*, *Shh* after exposure to SAG and SANT-75. (C) Relative expression levels of *Gli1*, *Ptc*, *Shh* after exposure to SAG and cyclopamine. (D) Timeline of the experimental procedures used in (E). Light irradiation at 4 J/cm^2 was followed by a 6 h incubation and cells were then used for RT-PCR and MTT assay. (E) Relative expression levels of *Gli1* in NIH3T3 cells exposed to NVOC-SANT-75 and light. The concentration of compound 4, SAG, SANT-75 and NVOC-SANT-75 were as follows: $1 \mu\text{M}$, 100 nM , $1 \mu\text{M}$, $1 \mu\text{M}$ respectively. $N = 3$, $*p < 0.05$. (F) MTT assay revealed no cytotoxicity in any of the conditions assayed.

but cells gradually stop proliferating and differentiate into neurons when cultured in vitro because there is an insufficiency in Hh ligands to maintain the activity of the Hh pathway. To maintain the background Hh signaling level, cells were treated with SAG throughout these experiments. At 24 h after plating, cells were treated with SANT-75 or NVOC-SANT-75 and exposed to light. At 48 h after plating, the cells were fixed, and immunostaining was performed (Fig. 3A). When we treated cells with NVOC-SANT-75 without light irradiation, the percentage of proliferating cells did not change compared to the DMSO treated control. However, when cells were treated with SANT-75 or NVOC-SANT-75

and exposed to light, the percentage of Ki67 positive cells decreased significantly. This suggests that light mediated inhibition of cellular proliferation was achieved by NVOC-SANT-75 (Fig. 3B, C).

To check if NVOC-SANT-75 altered neuronal differentiation, we quantified the percentage of cells with neurites in each group (Fig. 3D, E) using Tubb3 immunostaining. The percentages of Ki67 positive cells with neurites was low while there was a significant increase in neurite outgrowth for Ki67 negative cells. This was not disturbed by SANT-75 or NVOC-SANT-75 with light exposure. Next, we quantified the length of the neurites in the Ki67 positive cells and negative cells. This analysis

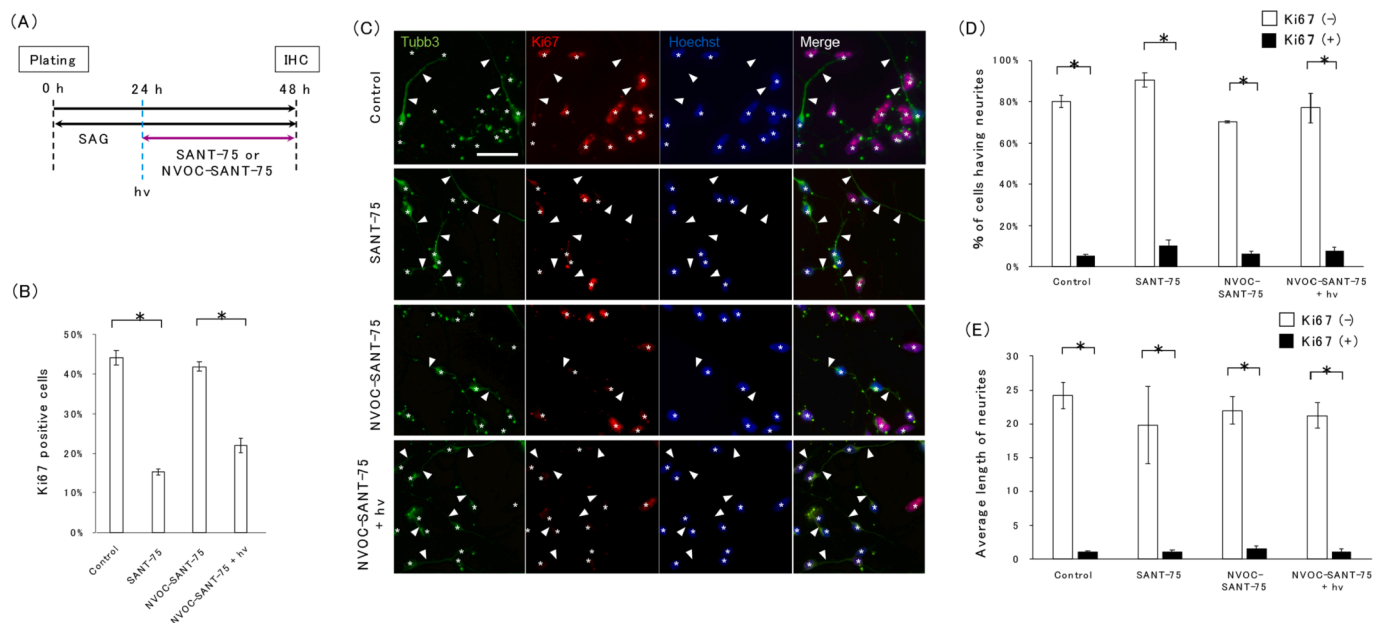


Fig 3. Control of proliferation and differentiation in mouse cerebellar granule neurons following treatment with NVOC-SANT75. (A) Timeline of the experimental procedures used in these assays. (B) Percentage of Ki67 positive cells under each condition 48 h after plating. $N = 3$, $*p < 0.05$. (C) Immunofluorescent images of mouse cerebellar granule neurons at 48 h after treatment as labeled. Scale bar: 20 μm . Asterisks indicate cell bodies and arrows indicate neurites. (D) Percentage of Ki67 positive and Ki67 negative cells with neurites. In all tested conditions, Ki67 negative cells have the higher percentage of cells with neurites. $N = 3$, $*p < 0.05$. (E) Average length of the neurites in Ki67 positive and negative cells. In all tested conditions, Ki67 negative cells have longer neurites than Ki67 positive cells. $N = 3$, $*p < 0.05$.

also revealed that there was no significant difference in the length of the neurites, indicating that NVOC-SANT-75 treatment and light irradiation did not negatively impact the differentiation of mouse granule neurons and showed no unexpected effects. Taken together, these data suggest that NVOC-SANT-75 not only modulates Hh signaling activity in immortal cancer cell lines but can also modulate the downstream differentiation of target cells without any apparent negative effects.

Many Hh signaling inhibitors have been developed as anti-cancer agents against Hh-dependent cancers.^{24,25} However, side effects such as muscle spasms, hair loss, and fatigue have been reported. Light-mediated treatments, including near-infrared photodynamic therapy and photoimmunotherapy, kill cancer cells in the light-irradiated region. By producing light activatable therapeutic compounds we can increase the clinical doses used at treatment to maximize the drug efficacy, while minimizing the side effects. However, because photodynamic therapy and photoimmunotherapy use near-infrared dyes that release reactive oxygen upon light irradiation, they are not cell type-specific and can potentially kill the surrounding healthy cells. By applying a protective group with absorption at longer wavelengths to our compound, it is expected that we could apply this candidate drug for cell type-specific light-mediated treatment.

3. Conclusion

In conclusion, we synthesized and evaluated a novel caged Hh signaling inhibitor, NVOC-SANT-75. The NVOC group entirely suppressed the inhibitory activity of SANT-75 against the Hh signaling pathway. photoirradiation released the NVOC group from the main active moiety, releasing SANT-75 in a precisely controlled manner. NVOC-SANT-75 is expected to be a useful tool for studying the physiological importance of the Hh signaling pathway, as well as a candidate for light-mediated therapy reagent.

4. Experimental section

4.1. Synthesis of SANT-75 and NVOC-SANT-75

4.1.1. Materials and analytical method

Compounds 1–4 and SANT-75 were synthesized as previously described.^{1,16} The reagents and solvents were purchased from commercial supplier as follows: 3-(Pyridin-4-yl)benzaldehyde was purchased from Sigma Aldrich; *N*-Boc,trans-1,4-cyclohexanediamine was purchased from Combi-Blocks; 3-chlorobenzo[*b*]thiophene-2-carbonyl chloride, iodopropane, NaBH_4 and NaH were purchased from Tokyo Kasei Co. Ltd. Chloroform, methanol, dichloromethane, ethyl acetate, acetonitrile, acetone, hexane, triethylamine, Na_2CO_3 and Mg_2SO_4 were purchased from Kanto Chemical. Co. Ltd. In addition, reagents and solvent were used as received without further purification. Reverse-phase HPLC was performed using a COSMOSIL 5C¹⁸-AR-II packed column (Nacalai Tesque Co. Ltd, 4.6 mm.I.D \times 250 mm) with a PU-2080 plus intelligent HPLC pump (Jasco).

The structural identities of the compounds were characterized by standard analytical methods, including ¹H NMR and ESI-MS spectroscopy. NMR spectra were recorded using an Advanced 600 instrument (Bruker) or an ECS 400 MHz NMR spectrometer (JEOL). ESI mass spectra were recorded using a Bruker MicroTOF II Nac.

4.1.2. Synthesis of compound 1

We mixed pyridinyl benzaldehyde (504 mg, 2.75 mmol, 1 eq) in dry methanol (30 mL) with Boc,trans-1,4-cyclohexanediamine (604 mg, 2.82 mmol, 1.02 eq), and the mixture was stirred on ice for 30 min. We then added NaBH_4 (332 mg, 8.78 mmol, 3.2 eq) and stirred on ice for 1 h at room temperature. This reaction was completed by adding saturated aqueous Na_2CO_3 (5 mL), and then extracting this mixture using chloroform (30 mL \times 3). The combined organic layer was dried over Mg_2SO_4 , and the solvent was removed under vacuum. The residue was purified by silica gel column chromatography (DCM/MeOH = 10:1) yielding purified compound 1. Yield: 82% (857 mg).

¹H NMR (600 MHz, CDCl_3) δ (ppm) 8.65 (d, Ar-H, 2H), 7.60–7.38 (m,

Ar-H, 5H), 4.40 (br, —NH—, 1H), 3.88 (s, —CH₂—, 2H), 3.43 (br, —CH—, 1H), 2.53–2.46 (m, —CH—, 1H), 2.04–1.99 (m, —CH₂—, 4H), 1.44 (s, —CH₃, 9H), 1.27–1.11 (m, —CH₂—, 4H).

4.1.3. Synthesis of compound 2

Compound 1 (857 mg, 2.24 mmol, 1 eq) was mixed with 3-chlorobenzo[b]thiophene-2-carbonyl chloride (569 mg, 2.46 mmol, 1.1 eq) in dichloromethane (20 mL), and then supplemented with dry Et₃N (750 μL, 5.3 mmol, 2.4 eq) and stirred at room temperature overnight. Both the solvent and Et₃N were removed under vacuum, and the residue was purified by silica gel column chromatography (Acetone: Hexane = 1:1) to give compound 2. Yield: 78% (1.00 g).

¹H NMR (600 MHz, CDCl₃) δ (ppm) 8.65 (s, Ar-H, 2H), 7.83–7.24 (m, Ar-H, 10H), 4.81 (s, —CH₂—, 2H), 4.65–4.24 (m, —CH—, 1H), 3.77 (s, —CH—, 1H), 3.29 (s, —CH—, 1H) 2.08–1.78 (m, —CH₂—, 4H), 1.64–1.61 (m, —CH₂—, 2H), 1.36 (s, —CH₃—, 9H), 1.03–0.93 (m, —CH₂—, 2H).

4.1.4. Synthesis of SANT-75

Compound 2 (90.1 mg, 156.4 μmol, 1 eq) in dry DMF was added to a catalytic amount of water (5 μL) and stirred on ice for 1 h. NaH (60 mg, 1.5 mmol, 10 eq) was then added and stirred on ice for an additional 1 h. This mixture was then supplemented with iodopropane (45 μL, 0.463 mmol, 1.9 eq), and the reaction mixture was stirred at room temperature overnight. This reaction was completed by adding saturated aqueous NaHCO₃ (10 mL), and the this mixture was then extracted with ethyl acetate (20 mL × 3), and the combined organic layer was dried using MgSO₄. The solvent was removed under vacuum, and resuspended in 4 M HCl ethyl acetate (10 mL) and stirred at room temperature for 30 min. The solvent was removed under vacuum, and the residue was purified by gradient silica gel column chromatography (chloroform: MeOH = 10:0 to chloroform: MeOH = 10:1) to give SANT-75. Yield: 33% (27.1 mg).

¹H NMR (600 MHz, DMSO-*d*₆) δ (ppm) 8.92 (s, Ar-H, 2H), 8.23–7.59 (m, Ar-H, 10H), 4.82 (s, —CH₂—, 2H), 3.61–3.55 (m, —CH—, 1H), 2.89 (s, —CH₂—, 2H), 1.91–1.76 (m, —CH₂—, 8H), 1.52–1.44 (m, —CH₂—, 2H), 1.27–1.16 (m, —CH₃—, 3H).

4.1.5. Synthesis of NVOC-SANT-75

We took a solution of SANT-75 (10.0 mg, 19.2 μmol, 1 eq) and compound 3 (14.7 mg, 28.2 μmol, 1.4 eq) in DMF (1 mL) and added Et₃N (50 μL) and then mixed them by stirring at room temperature overnight. Then we added 10 mL of water and extracted with ethyl acetate three times. The solvent was then removed under vacuum, and the residue was placed in 5 mL 4 M HCl acetic acid and stirred for 40 min at room temperature. The solvent was removed under vacuum and the residue was purified by silica gel chromatography (chloroform/MeOH = 10:1) and the corresponding fraction were collected. The solvent was removed under vacuum to give a pale yellow oil. The residue was further purified by high-performance liquid chromatography (C¹⁸-AR-II column, 4 mL/min, 0 min CH₃CN: H₂O = 5: 95, 15 min 100 : 0, 25 min 100 : 0). Yield 10% (2.34 mg).

¹H NMR (400 MHz, DMSO-*d*₆): δ (ppm) 8.68–8.59 (m, Ar-H, 2H), 8.17 (d, *J* = 9.1 Hz, Ar-H, 1H), 7.91 (d, *J* = 7.2 Hz, Ar-H, 1H), 7.79–7.49 (m, Ar-H, 9H), 6.06 (s, —CH—, 1H), 4.85 (s, —CH₂—, 2H), 4.05 (t, *J* = 7.2 Hz, —CH₂—, 2H), 3.84 (s, —CH₃, 3H), 3.74 (s, —CH—, 1H), 2.68–2.66 (m, —CH—, 1H), 2.38–2.35 (m, —CH₂—, 2H), 1.97–1.92 (m, —CH₂—, 2H), 1.96–1.76 (m, —CH₂—, 4H), 1.59–1.34 (m, —CH₂—, 4H), 1.35 (s, —CH₂—, 2H), 1.24 (s, —CH₃, 3H), 0.88–0.84 (m, —CH₃, 3H).

MS (ESI) *m/z* [M+H]⁺ calc 843.2825 found 843.2831. Purity: >99% (by HPLC analysis).

4.2. Photochemical characterization of NVOC-SANT-75

SANT-75 and NVOC-SANT-75 were dissolved in a 10% (v/v) DMSO/PBS solution. UV-Vis spectra were measured using Nanodrop spectrophotometer (Thermo Fisher). 1 mM NVOC-SANT-75 solution was

irradiated with 365 nm light at 0–8 J/cm² using a Xenon light source with a 365 nm bandpass filter (Max303, Asahi Spectra). Light intensity was determined using an illuminometer (UIT-201, Ushio). The light intensity was measured before each experiment. Each sample was analyzed using high performance liquid chromatography (5-C18-AR-II column, 0 min CH₃CN: H₂O = 5:95 to 8 min 30:70 to 15 min 0:100, monitored by 270 nm). Each peak was collected, and its molecular identity was confirmed by ESI-MS.

4.3. NIH3T3 cell culture

NIH3T3 cells were cultured in DMEM containing 10% calf serum, penicillin–streptomycin, and L-glutamine. NIH3T3 cells were split at a 1:5 ratio every three days. Cells were seeded on 12 well plates at 0.3x10⁶ cells/well and incubated for 48 h until confluent. Before stimulation, cells were starved in DMEM medium without calf serum for 24 h. Stimulation was performed by adding an appropriate amount of SAG and NVOC-SANT-75. After adding the drugs, photo irradiation was conducted using an LED light (EXF-UV, BioTools). Light intensity was determined using an illuminometer (UIT-201 with a 365 nm module, Ushio), and exposed to 4 J/cm² total irradiation. After additional 6 h incubation, total RNA was extracted and used for further analysis.

4.4. RT-PCR analysis

Total RNA was extracted using the TriPure Isolation Reagent Kit (11667165001, Roche Diagnostics). cDNA was synthesized using Superscript IV reverse transcriptase (Invitrogen) according to the manufacturer's protocol. RT-PCR was performed using the KAPA SYBR Fast qPCR kit (KAPA Biosystems) and CFX Connect (Bio-Rad). Expression levels were normalized against GAPDH which acts as the house keeping gene in these assays.

Primer sequence

GAPDH

fwd 5' GTTGTCTCTCGACTTCA 3'

rev 5' GGTGGTCCAGGGTTTCTTA 3'

Gli1

fwd 5' CTTCAAGGCCCAATACATGCTG 3'

rev 5' GCGTGAATAGGACTTCCGACA 3'

4.5. Mouse granule cell analysis

The cerebela tissues were removed from P6 ICR mice and then subjected to dissociation were conducted according to the previously described protocol with minor modifications. The cell culture surfaces were coated with Matrigel GFR (1:50 dilution with DMEM/F12) for 1 h at room temperature. 24 h after plating, cells were treated with SAG (100 nM) and NVOC-SANT-75 (100 nM), and light irradiation was conducted (4 J/cm²) from an LED light (EXF-UV, BioTools). The following antibodies were used in this analysis: a rabbit anti *Tubulin beta III* antibody (5H16, ZooMAb, Sigma, 1:1000). Anti-*Ki67* antibody (CST, D2H10, 1:1000).

For counting stained nuclei, ImageJ software was used. The background was subtracted, and the threshold was set to produce binary images. Images were processed using a watershed tool to separate the neighboring cells. Then, these processed images were analyzed using the particle tools. Particles larger than 1 μm were counted as individual nuclei. For neurite analysis, the length was evaluated manually with the line tool.

Author contribution

R.M. and Y.I. conceived and designed the experiments. R.M. performed the experiments and analyzed the data. R.M., A.O., and T.M. designed and planned the synthesis and characterization of the compounds. R.M. and Y.I. wrote the manuscript.

Funding

This work was supported in part by the Japan Society for the Promotion of Science (R.M.), the Ministry of Education, Culture, Sports, Science and Technology (MEXT) with a Grant-in-Aid for Scientific Research on Innovative Areas in the “Nascent Chain Biology” category (17H05661), the Japan Society for the Promotion of Science (JSPS) with a Grant-in-Aid for a Challenging Research (Pioneering) (20K20643), and the Grant-in-Aid for Transformative Research Areas (B) (20H05786), AMED-CREST, AMED (JP20gm1410001), Institute for AI and Beyond, Casio Science Promotion Foundation, TRI UTokyo, and Koyanagi Foundation (Y.I.).

Declaration of Competing Interest

The authors declare that they have no known competing financial interests or personal relationships that could have appeared to influence the work reported in this paper.

Acknowledgement

We thank Albert H. Kim, Kei Murata and Kazuyuki Ishii for their helpful advice around our experiments. We thank Kenichi Hatanaka and Kosaku Okuyama for their help obtaining the NMR data.

References

- Samadani AA, Norollahi SE, Rashidy-Pour A, et al. Cancer signaling pathways with a therapeutic approach: an overview in epigenetic regulations of cancer stem cells. *Biomed Pharmacother.* 2018;108:590–599. <https://doi.org/10.1016/j.biopha.2018.09.048>.
- Rubin LL, de Sauvage FJ. Targeting the Hedgehog pathway in cancer. *Nat Rev Drug Discov.* 2006;5:1026–1033. <https://doi.org/10.1038/nrd2086>.
- Varjosalo M, Taipale J. Hedgehog: functions and mechanisms. *Genes Dev.* 2008;22:2454–2472. <https://doi.org/10.1101/gad.1693608>.
- Briscoe J, Théron pp. The mechanisms of Hedgehog signalling and its roles in development and disease. *Nat Rev Mol Cell Biol.* 2013;14:418–431. <https://doi.org/10.1038/nrm3598>.
- Fujii K, Miyashita T. Gorlin syndrome (nevoid basal cell carcinoma syndrome): Update and literature review. *Pediatr Int.* 2014;56:667–674. <https://doi.org/10.1111/ped.12461>.
- Kugler MC, Joyner AL, Loomis CA, Munger JS. Sonic hedgehog signaling in the lung: from development to disease. *Am J Respir Cell Mol Biol.* 2015;52:1–13. <https://doi.org/10.1165/rcmb.2014-0132TR>.
- Yang L, Wang LS, Chen X, et al. Hedgehog signaling activation in the development of squamous cell carcinoma and adenocarcinoma of esophagus. *Int J Biochem Mol Biol.* 2012;3:46–57.
- Gu D, Schlotman KE, Xie J. Deciphering the role of hedgehog signaling in pancreatic cancer. *J Biomed Res.* 2016;30:353–360. <https://doi.org/10.7555/JBR.30.20150107>.
- Gonnissen A, Isebaert S, Hausermans K. Hedgehog signaling in prostate cancer and its therapeutic implication. *Int J Mol Sci.* 2013;14:13979–14007. <https://doi.org/10.3390/ijms140713979>.
- Riobo-Del Galdo N, Lara Montero Á, Wertheimer E. Role of Hedgehog Signaling in Breast Cancer: Pathogenesis and Therapeutics. Vol 8; 2019. <https://doi.org/10.3390/cells8040375>.
- Machado MV, Diehl AM. Hedgehog signalling in liver pathophysiology. *J Hepatol.* 2018;68:550–562. <https://doi.org/10.1016/j.jhep.2017.10.017>.
- Theunissen JW, De Sauvage FJ. Paracrine hedgehog signaling in cancer. *Cancer Res.* 2009;69:6007–6010. <https://doi.org/10.1158/0008-5472.CAN-09-0756>.
- Ruat M, Hoch L, Faure H, Rognan D. Targeting of smoothened for therapeutic gain. *Trends Pharmacol Sci.* 2014;35:237–246. <https://doi.org/10.1016/j.tips.2014.03.002>.
- Ellis-Davies GCR. Caged compounds: photorelease technology for control of cellular chemistry and physiology. *Nat Methods.* 2009;4:619–628. <https://doi.org/10.1038/nmeth1072>. Caged.
- Hess GP, Lewis RW, Chen Y. Caged neurotransmitters and other caged compounds: design and application. *Cold Spring Harb Protoc.* 2014;2014:1027–1039. <https://doi.org/10.1101/pdb.top084152>.
- Misawa R, Minami T, Okamoto A, Ikeuchi Y. A light-inducible hedgehog signaling activator modulates proliferation and differentiation of neural cells. *ACS Chem Biol.* 2020;15:1595–1603. <https://doi.org/10.1021/acscchembio.0c00195>.
- Yang H, Xiang J, Wang N, et al. Converse conformational control of smoothened activity by structurally related small molecules. *J Biol Chem.* 2009;284:20876–20884. <https://doi.org/10.1074/jbc.M807648200>.
- Deshpande I, Liang J, Hedeem D, et al. Smoothened stimulation by membrane sterols drives Hedgehog pathway activity. *Nature.* 2019. <https://doi.org/10.1038/s41586-019-1355-4>.
- Klán P, Solomek T, Bochet CG, et al. Photoremovable protecting groups in chemistry and biology: reaction mechanisms and efficacy. *Chem Rev.* 2013;113:119–191. <https://doi.org/10.1021/cr300177k>.
- Corrales JMD, Rocco GL, Blaess S, Guo Q, Joyner AL. Spatial pattern of sonic hedgehog signaling through Gli genes during cerebellum development. *Development.* 2004;131:5581–5590. <https://doi.org/10.1242/dev.01438>.
- De Luca A, Cerrato V, Fucà E, Parmigiani E, Buffo A, Leto K. Sonic hedgehog patterning during cerebellar development. *Cell Mol Life Sci.* 2016;73:291–303. <https://doi.org/10.1007/s00018-015-2065-1>.
- Hynes AM, Giles RH, Srivastava S, et al. Murine Joubert syndrome reveals Hedgehog signaling defects as a potential therapeutic target for nephronophthisis. *Proc Natl Acad Sci U S A.* 2014;111:9893–9898. <https://doi.org/10.1073/pnas.1322373111>.
- Lee HY, Greene LA, Mason CA, Manzini MC. Isolation and culture of post-natal mouse cerebellar granule neuron progenitor cells and neurons. *J Vis Exp.* 2009;23:20–23. <https://doi.org/10.3791/990>.
- Rimkus TK, Carpenter RL, Qasem S, Chan M, Lo HW. Targeting the sonic hedgehog signaling pathway: review of smoothened and GLI inhibitors. *Cancers (Basel).* 2016; 8:1–23. <https://doi.org/10.3390/cancers8020022>.
- Sekulic A, Von Hoff D. Hedgehog pathway inhibition. *Cell.* 2016;164:831. <https://doi.org/10.1016/j.cell.2016.02.021>.